AD-A092 572 NAVAL RESEARCH LAB WASHINGTON DC F/G 9/1
EFFECTS OF VELOCITY SPREAD AND WALL RESISTIVITY ON THE GAIN AND--ETC(U)
NOV 80 Y Y LAU, K R CHU, L BARNETT
UNCLASSIFIED NRL-MR-4304 NL

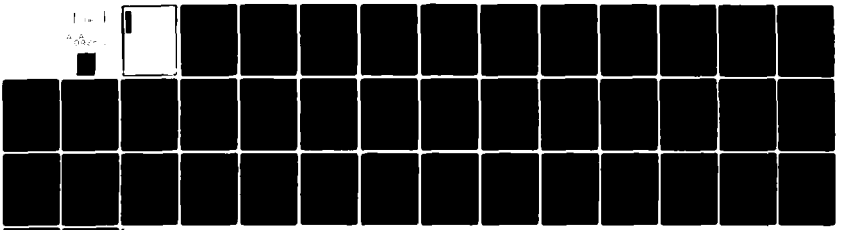

END
DATE FILMED
1-81
DTIC

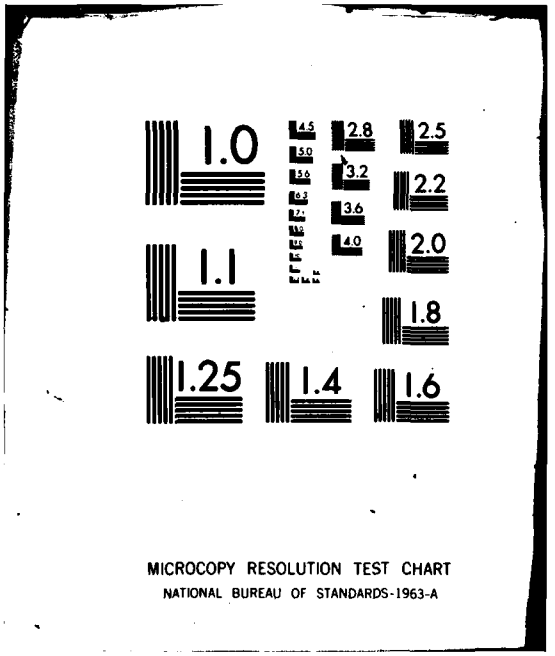
1.0
1.1
1.25
1.4
1.6
1.8
2.0
2.2
2.5
2.8
3.2
3.6
4.0
4.5
5.0
5.6
6.3
7.1
MICROCOPY RESOLUTION TEST CHART
NATIONAL BUREAU OF STANDARDS-1963-A

SECURITY CLASSIFICATION OF THIS PAGE (When Data Entered)

(9) **REPORT DOCUMENTATION PAGE**

READ INSTRUCTIONS BEFORE COMPLETING FORM

1. REPORT NUMBER: NRL Memorandum Report 4304	2. GOVT ACCESSION NO.: AD-A092 572
3. RECIPIENT'S CATALOG NUMBER	
4. TITLE (and Subtitle): (6) EFFECTS OF VELOCITY SPREAD AND WALL RESISTIVITY ON THE GAIN AND BANDWIDTH OF THE GYROTRON TRAVELLING-WAVE AMPLIFIER*	5. TYPE OF REPORT & PERIOD COVERED: Interim report on a continuing NRL problem
	6. PERFORMING ORG. REPORT NUMBER
7. AUTHOR(s): (10) Y.Y. Lau*, K.R. Chu, and L. Barnett**	8. CONTRACT OR GRANT NUMBER(s): (11) 12 Nov 80
9. PERFORMING ORGANIZATION NAME AND ADDRESS: Naval Research Laboratory, Washington, D.C. 20375 (12) 42	10. PROGRAM ELEMENT, PROJECT, TASK AREA & WORK UNIT NUMBERS: Program Element - 62762N; Project No. XF62 581007; NRL Problem 67-0863-0-0
11. CONTROLLING OFFICE NAME AND ADDRESS: Naval Electronic Systems Command, Washington, D.C. 20360	12. REPORT DATE: November 12, 1980
	13. NUMBER OF PAGES: 41
14. MONITORING AGENCY NAME & ADDRESS(if different from Controlling Office): (14) NRL-MR-4304	15. SECURITY CLASS. (of this report): Unclassified
	15a. DECLASSIFICATION/DOWNGRADING SCHEDULE

16. DISTRIBUTION STATEMENT (of this Report)

Approved for public release; distribution unlimited.

(16) F62581

17. DISTRIBUTION STATEMENT (of the abstract entered in Block 20, if different from Report)

(17) XF625819971

18. SUPPLEMENTARY NOTES

*Science Applications, Inc., McLean, VA

**B-K Dynamics, Rockville, MD

19. KEY WORDS (Continue on reverse side if necessary and identify by block number)

Gyro-TWA
Cyclotron Harmonic
Velocity Spread

20. ABSTRACT (Continue on reverse side if necessary and identify by block number)

The small signal gain and bandwidth of the gyrotron travelling-wave amplifier (gyro-TWA) operating at the fundamental cyclotron harmonic are examined. The analytical and numerical studies focus on the effects of velocity spread in the electron beam and of a distributed wall resistivity in the waveguide. It is found that wall resistivity reduces the forward gain of the amplifier only by an amount approximately equal to 1/3 of the corresponding cold tube loss. Significant increase in bandwidth may result, under certain conditions, from the presence of wall

(Continued)

DD FORM 1 JAN 73 1473 EDITION OF 1 NOV 65 IS OBSOLETE
S/N 0102-014-6601

25195 Ø

20. Abstract (Continued)

resistivity. A moderate amount (5-10%) of velocity spread does not reduce the peak gain significantly in general, but may reduce the bandwidth by an amount depending on the applied magnetic field. Based on considerations of such factors as power, stability, gain, bandwidth, and efficiency, operating parameters for the gyro-TWA are suggested.

CONTENTS

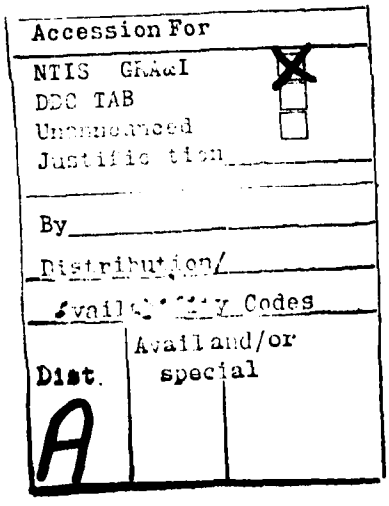

EFFECTS OF VELOCITY SPREAD AND WALL RESISTIVITY ON THE GAIN AND BANDWIDTH OF THE GYROTRON TRAVELLING-WAVE AMPLIFIER

I. INTRODUCTION

The onset of oscillations at a relatively low current level remains a major obstacle in the development of high power gyrotron travelling wave amplifier (gyro-TWA)[1,2]. Analogous to the conventional travelling wave tube, it has been experimentally shown that the introduction of wall loss, either in the form of a lumped or distributed loss[3], may render the gyro-TWA stable against oscillations resulted from reflections. Parallel theoretical studies[4] also reveal that a small wall resistivity may reduce the danger of exciting an absolute instability,[5] whose presence can lead to oscillations even in the absence of reflections. While wall resistivity may stabilize the amplifier against both types of oscillations, it may also modify the gain and the bandwidth. On the other hand, there is always the interesting possibility that it may also lead to some type of resistive instability which would not exist if there is no wall resistivity. Thus, in this work, we study in detail the effects of a distributed wall resistivity on the gain and bandwidth of the gyro-TWA, with the velocity spread in the electron beam accounted for. Previously[1,6], the effect of velocity spread has been studied in the absence of wall resistivity. Here, we study the combined effects of the wall resistivity and velocity spread with emphasis on the former.

Under the realistic assumptions that the skin depth δ of the wall material is much less than the wall thickness and the wall radius r_w, we generalize the dispersion relation derived earlier[7] to include the effect of wall resistivity and of velocity spread. We analyze the gain curves over a wide range of parameters. The principal results are summarized as follows.

The presence of a small resistivity (e.g., $\delta/r_w = 0.0026$, as in the NRL experiments), only slightly reduces the gain of the amplifier. More specifically, the reduction in gain is approximately 1/3 of the

Manuscript submitted August 5, 1980.

cold-tube loss for frequencies in the neighborhood of the grazing intersection. This result may be paraphrased as that the resistive wall is 3 times as effective in damping the backward waves reflected from the end of the waveguide than the forward amplifying waves, leading to the distinct possibility that wall resistivity may stabilize the amplifier without significantly reducing its gain. (Recall in this regard that the resistive wall may also stabilize the absolute instability, as mentioned earlier).

Of equal interest is our finding that wall resistivity can increase the bandwidth for realistic values of δ/r_w. This increase in bandwidth, which is quite substantial when the applied magnetic field is maintained exactly at the grazing value, results primarily from the leveling of the gain curve. The bandwidth is less sensitive to wall resistivity if the magnetic field is below the grazing value. The presence of wall resistivity also broadens the unstable band in the frequency spectrum: growth of waves below the waveguide cutoff frequency is found possible, leading to some optimism that very wide band amplifier may be realized.

A modest amount of velocity spread, say, on the order of 10 per cent, does not reduce the peak gain significantly. However, the bandwidth may be significantly reduced. The reduction in bandwidth is most noticeable when the magnetic field is exactly at the grazing value. For a slightly lower value of magnetic field, the reduction in bandwidth is minimal, even at a current level as high as 10 amps.

The extensive numerical study of gain and bandwidth points to the following optimum design parameters: A beam current on the order of 10 amps, an applied magnetic field about 2% below the grazing value, a wall resistivity with a skin depth about five thousandth of the wall radius. For a gyro-TWA with such design parameters, a gain on the order of 3.5 db/wavelength with a bandwidth of approximately 4 per cent could be achieved. Such an amplifier may operate stably with significant efficiency.

In keeping with the operation of the amplifier, namely, amplification of a signal of frequency ω, in this paper, we shall calculate the complex axial wavenumber k_z as a function of (real) ω from the

dispersion relation. We should remark that in so doing, care must be exercised to obtain and to interpret the gain curve, especially when the current exceeds the threshold value for the onset of absolute instabilities.[4] The proper branch of the solution must be chosen [cf. Ref. (5), p. 38]. On the other hand, calculations of complex ω for real values of k_z might easily be misused in connection with amplifiers [cf. Ref. (5), p. 167].

In Section II, we shall formulate the dispersion relation including the effect of wall resistivity and of the velocity spread in the electron beam. The numerical results are presented in Section III. The major results and implication are discussed in Section IV.

II. FORMULATION

The inclusion of a small, but finite wall resistivity in the waveguide requires some modification of the derivation of the dispersion relationship. Considerable simplification results when two assumptions are introduced: (1) The beam is sufficiently tenuous that the wave with which it interacts is primarily the vacuum field supported by the (lossy) waveguide; (2) The thickness, as well as the inner radius r_w of the resistive wall are much larger than the skin depth δ associated with the wall material.

The first assumption was adopted in virtually all literature on gyrotron. The excellent agreement between experiments and the theory developed under this assumption leaves little doubt regarding its validity. Implied also in this assumption is that the beam mode and the waveguide mode are close to synchronism. One should take precaution, therefore, if the present formalism is to be extrapolated to explore the possibility of designing an extremely wideband amplifier, even though such a possibility is potentially attractive. The second assumption is also generally valid for any realistic gyro-TWA experiment. For example, in the planned NRL experiments $r_w = .533$ cm, $\delta \simeq 1.4 \times 10^{-3}$ cm at 35 GHz.[3] Thus $\delta/r_w \cong 2.6 \times 10^{-3}$, an extremely small quantity compared with unity.

Our calculation of the dispersion relationship follows closely with Chu, Drobot, Szu, and Sprangle.[7] First, the vacuum fields of the TE_{on} mode in a cylindrical lossy waveguide are

$$B_z^{(1)} = J_0(\alpha_n r) \exp(ik_z z - i\omega t) \tag{1}$$

$$B_r^{(1)} = \left[-i\frac{k_z}{\alpha_n}\right] J_1(\alpha_n r) \exp(ik_z - i\omega t) \tag{2}$$

$$E_\theta^{(1)} = -\omega B_r^{(1)}/k_z c. \tag{3}$$

Here, J_0 and J_1 are Bessel functions of order zero and one. As will be shown in Appendix A, the characteristic radial wavenumber α_n is given by the equation

$$\frac{\delta}{r_w}\left[\frac{1-i}{2}\right]\zeta J_0(\zeta) = J_1(\zeta), \tag{4}$$

where

$$\zeta \equiv \alpha_n r_w \equiv r_w\sqrt{\frac{\omega^2}{c^2} - k_z^2}. \tag{5}$$

In the limit of small δ/r_w, the approximate solution to Eq. (4) is

$$\zeta = \zeta_{on}\left[1 + \frac{\delta}{r_w}\frac{(1-i)}{2}\right] \tag{6}$$

where ζ_{on} is the $n-$th non-trivial root of J_1, i.e., $\zeta_{on} = 3.832,\ 7.016,\ 10.173$, etc. When we denote $\alpha_{on} \equiv \zeta_{on}/r_w$, the slightly complex radial wavenumber reads

$$\alpha_n = \alpha_{on}\left[1 + \frac{\delta}{r_w}\frac{(1-i)}{2}\right]. \tag{7}$$

Note that

$$J_1(\alpha_n r_w)\begin{cases} = J_1(\alpha_{on} r_w) = 0, & \text{if } \delta = 0 \quad (8) \\ \neq 0, & \text{if } \delta \neq 0 \quad . \quad (9) \end{cases}$$

To make full use of the mathematical property of Bessel functions, let us define

$$r_w^* \equiv \frac{\alpha_{on} r_w}{\alpha_n} \cong r_w\left[1 - \frac{\delta}{r_w}\frac{(1-i)}{2}\right]. \tag{10}$$

Thus

$$J_1(\alpha_n r_w^*) = 0. \tag{11}$$

For ready comparison with the cold tube loss rate resulting from wall resistivity, we calculate the axial wavenumber k_z for the emply waveguide. From Eqs. (5) and (6), we find, for the empty waveguide, $k_z = k_{zE}$ where

$$k_{zE}^2 = k_{zo}^2 - \alpha_{on}^2 (1 - i) \frac{\delta}{r_w}, \tag{12}$$

with

$$k_{zo} \equiv \left[\frac{\omega^2}{c^2} - \alpha_{on}^2\right]^{1/2} \tag{13}$$

being the axial wavenumber of the corresponding lossless waveguide. Note that Eq. (12) is valid even if $k_{zo} = 0$. It will be used to calculate the attenuation rate of the waves in the cold tube due to the wall loss. On the other hand, measurements of attenuation rate for the cold tube at various frequencies may be used to determine the skin depth of the wall material by Eq. (12).

We now consider the interaction of the electron beam with the above electromagnetic waves. In the typical configuration of a gyro-TWA (Fig. 1), the electrons, forming an annular beam, are guided by a uniform magnetic field ($B_o\, e_z$). They move along helical trajectories. Ideally, all electrons have the same perpendicular velocity $v_{\perp o}$ and the same parallel velocity v_{zo}, with their guiding centers uniformly distributed on a surface of constant radius r_o (Fig. 1). The electromagnetic fields represented by Eqs. (1)-(3) induce a current perturbation in the beam. This response in the current has been computed by Chu[8] for the lossless waveguide by solving the linearized Vlasov equation. His calculation can readily be extended to the present case of a lossy waveguide because the field solutions $J_0(\alpha_n r)$ and $J_1(\alpha_n r)$ in Eqs. (1)-(3) are entire functions of $\alpha_n r$. In order that this perturbation current $J^{(1)}$ be consistant with the field solutions (1)-(3), they must be related by the Maxwell equations as follows:

$$\frac{1}{r}\frac{\partial}{\partial r}\left[r\frac{\partial B_z^{(1)}}{\partial r}\right] - k_z^2 B_z^{(1)} + \frac{\omega^2}{c^2} B_z^{(1)} = -\frac{1}{r}\frac{\partial}{\partial r}(rJ_\theta^{(1)}), \tag{14}$$

where $J_\theta^{(1)}$ is the θ component of the perturbation current. Strictly speaking, Eq. (14) is an integral-differential equation since $J_\theta^{(1)}$ is a functional of the fields which are to be solved self-consistently.

The first assumption introduced at the beginning of this section can now be used to simplify the formulation. By this assumption $B_z^{(1)}$ is given by Eq. (1). Multiply equation (14) by $rJ_0(\alpha_n r)$ and integrate the resultant equation from $r = 0$ to $r_w{}^*$. We then obtain

$$\left[\frac{\omega^2}{c^2} - k_z^2 - \alpha_n^2\right] = \frac{8\pi\alpha_n\, e^{-ik_z z+i\omega t}}{c\, r_w{}^{*2}\, J_0^2(\zeta_{on})} \int_0^{r_w{}^*} dr\; r\; J_\theta^{(1)}\; J_1(\alpha_n r) \tag{15}$$

where we have used equation (11) and α_n, $r_w{}^*$ are given by equations (7) and (10) respectively. This procedure is justified as all quantities in equation (14) are entire functions of r. For the same reason, the modified dispersion relation now reads

$$\begin{aligned}\frac{\omega^2}{c^2} - k_z^2 - \alpha_n^2 = \frac{-8\pi\nu}{\zeta_{on}^2 J_0^2(\zeta_{on})} \int_0^\infty p_\perp\, dp_\perp \int_{-\infty}^\infty dp_z g(p_\perp, p_z) \\ \cdot\left\{\frac{(\omega^2 - k_z^2c^2)p_\perp^2 H_s(\alpha_n r_0, \alpha_n r_L)}{\gamma^3 m^2 c^2(\omega - k_z v_z - s\Omega_c)^2}\right. \\ \left. - \frac{(\omega - k_z v_z) Q_s(\alpha_n r_0, \alpha_n r_L)}{\gamma(\omega - k_z v_z - s\Omega_c)}\right\}\end{aligned} \tag{16}$$

where $\Omega_c = eB_o/\gamma mc$, $r_L = v_\perp/\Omega_c$, $\nu \equiv Ne^2/mc^2$ is the dimensionless beam density parameter, N is the number of electrons per axial length, and the functions H_s and Q_s are defined by

$$H_s(x,y) \equiv [J_s(x)J'_s(y)]^2$$

and

$$\begin{aligned}Q_s(x,y) \equiv\; & 2H_s(x,y) + yJ'_s(y)J''_s(y)\{J_s^2(x)(1 + s^2/x^2) \\ & + [J'_s(x)]^2\} + 2s^2 J_s(x)J'_s(x)J'_s(y)[yJ'_s(y) \\ & - J_s(y)]/xy.\end{aligned}$$

In Eq. (16), $g(p_\perp, p_z)$ is an arbitrary function of the momentum $p_\perp$ and p_z satisfying $\int g(p_\perp, p_z)\, d^3p = 1$. The most suitable electron beams for the gyrotrons are those generated from a magnetron-type electron gun. Typically, such beams are characterized by a negligible energy spread, hence the velocity spread comes primarily from the pitch angle spread of the electron velocity. To model this kind of beam, we let

$$g(p_\perp, p_z) = K\, \delta(\gamma - \gamma_o) \exp\left[\frac{-(p_z - p_{zo})^2}{(\Delta p_z)^2}\right],$$

where K is a normalization constant and Δp_z is the mean axial velocity spread, and δ is the delta function of Dirac.

Equation (16) is identical in form with that for the lossless waveguide[1,6] except that α_n now has a small imaginary part, and that we have neglected the azimuthal modes. It incorporated two obvious physical effects of the wall resistivity: (a) its modification of the waveguide mode and hence (b) the modified beam-wave interaction as a result of the modification in the electromagnetic field. The first effect is represented by the complex α_n appearing in the LHS of Eq. (16) and the second effect by that in the RHS. In Appendix B, we show that the second effect is negligible in comparison with the first effect. Thus we may replace α_n by α_{on} in the right hand side of Eq. (16).

It is anticipated that wall resistivity should reduce the forward gain of the amplifier. Actually, the reduction in the gain is considerably less than that expected of the vacuum waveguide. In Appendix B, we estimate that the reduction in the gain by wall resistivity is approximately 1/3 of the cold tube loss (by resistivity) at the same frequency. This analytic result is supported by our numerical results. It may be regarded significant since it means that wall resistivity may stabilize the amplifier, by damping out any reflected signal from the end of the waveguide, without sacrificing the forward gain as significantly.

In Section III, we shall present numerical results for various combinations of δ/r_w, velocity spread, beam current and the applied magnetic field. The results are obtained from the full dispersion relationship (16), and from its modified form when velocity spread is present.

III. NUMERICAL EXAMPLES

The general dispersion relationship (16) is applicable to all cyclotron harmonics (s) and to all radial mode numbers (n). Thus, a huge parameter space needs to be explored for an exhaustive investigation of the performance of the gyro-TWA. To limit our studies of the effects of wall resistivity and

of velocity spread, we shall only examine the lowest cyclotron harmonic of the TE_{01} mode. Even then, four parameters need to be specified to obtain the gain curve. They are:

(a) the magnetic field B_0, in units of the grazing value B_G,

(b) the current I,

(c) the wall resistivity, measured by δ/r_w, and

(d) the velocity spread, measured by $\Delta p_z/p_{z0}$.

The magnetic field is said to assume the grazing value when the non-relativisitic electron cyclotron frequency equals to the cut-off frequency of the waveguide. The numerical examples obtained may then be used, after properly scaled, to predict the performance of the amplifier operated at higher harmonics and at higher order modes.

To facilitate comparison of results, at the expense of some duplications, we shall present our numerical calculations in three subsections. In each subsection, gain curves are given in which three of the four parameters mentioned above are held fixed and only the remaining one is allowed to vary. All gain curves are drawn with the same scale. The individual effects are thus placed in sharp focus. In Subsection a, in each graph of the gain curves, only the wall resistivity is varied. In Subsection b, only the velocity spread is varied and in Subsection c, only the current is varied. In all cases studied, we assume that $\beta_{\parallel} = 0.266$, $v_{\perp 0}/v_{\parallel 0} = 1.5$ and that the beam energy is 70 keV. These assumptions closely represent the NRL experiments.[1] We shall postpone to the next section for some general discussion of the role of resistivity in instabilities.

a. The Effect of Wall Resistivity

In this subsection, we present the gain curves in which the wall resistivity (δ/r_w) is allowed to vary. We shall plot the normalized spatial growth rate $\bar{k}_I \equiv -k_I r_w$ as a function of normalized frequency $\bar{\omega} \equiv \omega\, r_w/c$. For a lossless waveguide, $\bar{\omega}$ assumes the value 3.832 at the cutoff frequency and 3.975 at the grazing frequency. In both Figs. (2) and (3), we set $B/B_G = 1$ and $\Delta p_z = 0$. In Fig. (2),

$I = 1$ amp and in Fig. 3, $I = 3$ amps. Also shown in parentheses in these figures are the bandwidths, which represent the frequency range inside which the gain is within 85% of the peak value. It is seen from these two figures that the gain is not reduced by a significant amount as δ/r_w is raised from 0 to 0.0025 (again, in the NRL experiments, $\delta/r_w \simeq 0.0025$). If δ/r_w is further raised from 0.0025 to 0.01, which amounts to an increase of wall resistivity by a factor of 16, we see that the bandwidth significantly increases [c.f. Fig. 3] while the gain is not substantially reduced. In fact, if we compare the numerical value of this reduction in gain with the cold tube loss as determined from Eq. (12) [c.f. Fig. 4] the former is approximately 1/3 of the latter, over the useful bandwidth in the vicinity of the grazing frequency. This result is in qualitative agreement with the analytical study given in Appendix B. The sharp peak in the $\delta/r_w = 0$ curve in Fig. 3 is indicative of the presence of an absolute instability[4] in that case.

In Figs. 5-7, we include the effect of the velocity spread while the magnetic field is still maintained at the grazing level. It is again seen that the bandwidth increases with wall resistivity, and the forward gain is not reduced significantly.

In Fig. 8, we set $B/B_G = 0.98$, $I = 7$ amps, and $\Delta p_z = 0$. The bandwidth also increases with wall resistivity, but its dependence on resistivity is less sensitive than that in the case of exact grazing magnetic field. The slight decrease in bandwidth as δ/r_w changes from 0.005 to 0.01 as shown in this figure suggest the presence of resistive damping.

It is of interest to point out that even though the peak gain is reduced by wall resistivity, the unstable band of the amplifier is enlarged. Virtually, in all cases, the unstable band extends to frequencies below the cut-off frequency of the waveguide if wall resistivity is included, thus suggesting the presence of some resistive wall-induced instability. We shall comment on this dual role of resistivity in Section IV.

b. The Effect of Velocity Spread

In this subsection, we evaluate the effect of velocity spread on the gain and bandwidth of the gyro-TWA. In each figure, all parameters are held fixed except the velocity spread $\Delta p_z/p_{zo}$. We take the values of $\Delta p_z/p_{zo}$ to be 0, 7% and 15%. It is found that the velocity spread reduces the gain and bandwidth significantly when the magnetic field is maintained at the grazing level. On the other hand, when $B/B_G < 1$, velocity spread does not seem to reduce the gain nor the bandwidth to as a great extent, even at a high current level. [Of course, one might also worry that at a high current level, the beam quality may deteriorate and the velocity spread may increase].

In Figs. 9-11, we set $B/B_G = 1$, $I = 1$ amp, and let $\delta/r_w = 0$, 0.0025 and 0.1 respectively. We see that at this low current level, the presence of velocity spread reduces the gain and bandwidth quite significantly [c.f. Fig. 11]. This remains to be the case when the current is raised to 3 amps, as shown in Figs. 12-14, where we still set $B = B_G$..

If we lower the magnetic field, so that $B/B_G = 0.98$, [c.f. Figs. (15)-(17)], then the velocity spread has a lesser influence in the gain and in the bandwidth. In these figures, we have set $\delta/r_w = 0.0025$. A higher value of δ/r_w, such as 0.01 as used in Figs. 18-21, would permit the amplifier to operate stably at substantially higher current.[4] It is apparent from these figures that the bandwidth, as well as the gain, again does not greatly suffer from the presence of velocity spread.

c. The Effect of Increasing Current

Finally, we examine the dependence of gain and bandwidth on the current. When the current is sufficiently high, an absolute instability sets in. There would then be some ambiguity[5] regarding the proper solutions of the amplifying waves. Such an ambignity arises from the intersection of the branch cut in the ω plane with the real ω axis. It does not seem to pose a serious problem in the present study when the beam current exceeds the threshold current only by a moderate factor, such as 1.5. We have

exercised some care in choosing the correct solution, and we may refer to Ref. (4) for a detailed discussion of the absolute instability and for the calculation of the threshold current in the gyro-TWA.

Here, we report that while the gain increases with the current, as expected, the bandwidth decreases once the current exceeds the threshold value for the onset of absolute instability. This may be intepreted as the tendency of the system to respond mostly to a particular frequency, namely, the natural frequency of oscillation when the absolute instability is present, thereby leading to a narrow bandwidth that results from the sharp peak in the gain curve in the neighborhood of that natural frequency. These statements are corroborated in Figs. 22 and 23, where the gain curves tend to peak at the cutoff frequency (i.e., $\bar{\omega}_c = \omega_c r_w/c = 3.832$), which also is the frequency[4] for the onset of the absolute instability. From Ref. (4) the threshold current for parameters shown in Fig. 22 is 1.5 amps and that for Fig. 23 is 5.0 amps.

On the other hand, if the current is below the threshold value, then increasing the current would lead to the increase of both gain and bandwidth, as clearly indicated in Figs. 24-27. In these figures, we set $B/B_G = 0.98$ so that the threshold current is high[4]. The threshold current for both Figs. 24 and 25 is 5.5 amps and that for both Figs. 26 and 27 is 12 amps. The velocity spread in Fig. 24 is 7% and that in Fig. 25 is 15%. Figure 26 and Fig. 27 differ also only in velocity spread. The curves in Fig. 26 are hardly modified if the velocity spread in 7% instead of zero [c.f. Figs. 15-21].

IV. DISCUSSIONS

One thing that stands out among the numerical results is the dual role played by electrical resistivity: (a) in its reduction of the gain of the cyclotron maser instability and (b) in its excitation of amplifying waves in a regime where such amplification would have been impossible if the resistivity is absent. Such a dual role of dissipative effects is of common occurrence in physical systems with available free energy. If in such a system an instability of the reactive type[5] is already present even in the absence of dissipative effects, the introduction of dissipation would reduce the growth rate because it

takes away the free energy that drives the instability. On the other hand, if there is no instability in such a system in the absence of dissipation, the introduction of dissipative effects would lead to growth of waves, as dissipation would induce relaxation of the system which is on the verge of becoming unstable to begin with. Numerous examples of these phenomena can be found in the literature of classical mechanics, hydrodynamics, plasma physics, electron beam devices, astrophysics, etc.

The major results and their implication of the present study may then be summarized as follows:

(1) In terms of power, gain, bandwidth, efficiency, and stability, the gyro-TWA would achieve best overall performance when the magnetic field is maintained just slightly (say, 2%) below the grazing value. Stable operation with significant gain and bandwidth (such as 3-4 db per wavelength in gain and 4% in bandwidth) may be achieved at a current of 10 amps, or even higher, if $\delta/r_w \geqq 0.005$.

(2) Wall resistivity leads to a reduction in gain by an amount on the order of 1/3 of the cold tube loss. It leads to an increase in bandwidth when the magnetic field is maintained at the grazing value. If the magnetic field is below the grazing value, and if the current is low, the presence of wall resistivity may actually reduce the bandwidth. The latter may be regarded as an example of resistive damping.

(3) Velocity spread typical of present electron guns ($\Delta p_z/p_{z0} \simeq 5-10\%$) does not significantly reduce the peak gain. The underlying reason is that its effect enters in the combination $k_z^2(\Delta p_z)^2$ qualitatively and the amplifier reaches a peak gain when $\omega \simeq \omega_c$, at which k_z is small. At higher frequencies, k_z becomes sizable and the effect of velocity spread would then be important. Thus, the bandwidth may be significantly reduced, especially if the magnetic field is maintained at the grazing value.

(4) The gain and bandwidth of the amplifier are less sensitive to velocity spread or to resistivity when the magnetic field is below the grazing value. Thus, for stability of the

amplifier, we need a wall resistivity whose skin depth is on the order of $5 \times 10^{-3}\, r_w$. To reduce the deteriorating influence of the velocity spread on the bandwidth, the magnetic field should be maintained slightly below the grazing value. The current should be on the order of 10 amps, which is sufficiently high for gain and power, yet low enough to avoid oscillations. These arguments form the basis of the parameters quoted in the Abstract.

ACKNOWLEDGEMENT

We like to thank Drs. M. Baird, V. L. Granatstein and A. Drobot for discussions. This work is supported in part by NAVELEX, Task XF54581007.

REFERENCES

* Science Applications, Inc.

** B.-K. Dynamics

1. J.L. Seftor, V.L. Granatstein, K.R. Chu, P. Sprangle and M.E. Read, "The Electron Cyclotron Maser as a High-Power Travelling Wave Amplifier of Millimeter Waves," IEEE J. Quantum Electronics, Vol. QE-15, pp. 848-853 (1979).

2. L.R. Barnett, K.R. Chu, J.M. Baird, V.L. Granatstein, and A.T. Drobot, "Gain, Saturation, and Bandwidth Measurements of the NRL Gyrotron Travelling Wave Amplifier," IEDM Technical Digest, pp. 164-167 (Dec., 1979).

3. L.R. Barnett, et al., to be published. R.S. Symons, H.R. Jory, and S.T. Hegii, to be published.

4. Y.Y. Lau, K.R. Chu, L.R. Barnett and V.L. Granatstein, "Analysis of Oscillations in the Gyrotron Travelling-Wave Amplifier," to be published.

5. R.J. Briggs, *Electron Stream Interaction with Plasma*, MIT Press, Cambridge, Mass. (1964).

6. H.S. Uhm and R.C. Davidson, "Influence of Energy and Axial Momentum Spreads on the Cyclotron Maser Instability in Intense Hollow Electron Beams," Phys. Fluids, Vol. 22, pp. 1804-1810 (1979).

7. K.R. Chu, A.T. Drobot, H.H. Szu, and P. Sprangle, "Theory and Simulation of the Gyrotron Travelling Wave Amplifier Operating at Cyclotron Harmonics," IEEE Trans. MTT (April, 1980).

8. K.R. Chu, "Theory of Electron Cyclotron Maser Interaction in a Cavity at the Harmonic Frequencies," Phys. Fluids, Vol. 21, pp. 2354-2364 (1978).

Appendix A

DERIVATIONS OF FIELD PATTERNS IN A CYLINDRICAL LOSSY WAVEGUIDE

In this Appendix, we calculate the field patterns of the TE_{on} modes in an empty, cylindrical waveguide with a lossy wall. We shall assume that the skin depth δ of the wall is much less than the wall radius r_w, the wall thickness, and the free space wavelength c/ω. Thus, we consider two regions. Region I is the free space region: $0 < r < r_w$, inside which the electrical conductivity σ is zero. Region II is the wall region: $r_w < r < \infty$, where σ is large but finite.

It is well known that the z component of the magnetic field of the TE_{on} mode is governed by the Bessel equation

$$\left[\frac{1}{r}\frac{\partial}{\partial r}\left(r\frac{\partial}{\partial r}\right) + k_n^2\right] B_z^{(1)} = 0. \tag{A1}$$

In region I, $k_n^2 = k_{n1}^2$ where

$$k_{n1}^2 = \frac{\omega^2}{c^2} - k_z^2. \tag{A2}$$

Thus, the solution which is regular in this region is

$$B_z^{(1)}(r) = A\ J_0(k_{n1}r), \quad 0 \leqslant r < r_w, \tag{A3}$$

where A is an arbitrary constant and J_0 is the Bessel function of order zero.

In Region II, $k_n^2 = k_{n2}^2$, where

$$k_{n2}^2 = \frac{\omega^2}{c^2}\left[1 - \frac{\sigma}{i\omega\epsilon_o}\right] - k_z^2 \simeq i\omega\mu_o\sigma. \tag{A4}$$

Here, ϵ_o and μ_o are the permittivity and permeability of free space. In writing the last expression in (A4), we have assumed that the skin depth

$$\delta = \sqrt{\frac{2}{\omega\mu_o\sigma}} \tag{A5}$$

is much less than the free space wavelength c/ω. Using (A4) into (A1), and introducing the transformation

$$B_z^{(1)} = r^{-1/2}\,\phi, \tag{A6}$$

we rewrite equation (A1) for Region II as

$$\frac{d^2\phi}{dr^2} + \left[i\omega\mu_0\sigma + \frac{1}{4r^2}\right]\phi = 0, \quad r_w < r < \infty. \tag{A7}$$

The last term $1/4r^2$ is clearly small in comparison with $\omega\mu_0\sigma$ for all $r > r_w$ and hence is neglected. In order that the solution to (A7) is bounded as $r \to \infty$, we have

$$B_z^{(1)}(r) = r^{-1/2}\,\phi(r) \simeq B\,r^{-1/2}\,e^{-(1+i)r/\delta}; \quad r > r_w \tag{A8}$$

where B is an arbitrary constant. Two conditions are now imposed on the solutions (A3) and (A8) at the boundary $r = r_w$ separating the two regions:

$$B_z^{(1)}(r)\Big|_{r=r_w^-} = B_z^{(1)}(r)\Big|_{r=r_w^+} \tag{A9}$$

$$\frac{dB_z^{(1)}(r)}{dr}\Big|_{r=r_w^-} = \frac{dB_z^{(1)}(r)}{dr}\Big|_{r=r_w^+} \tag{A10}$$

Condition (A9) assures the continuity of the magnetic field and (A10) the continuity of the tangential electric field. Observe from Eq. (A8) that the variation of the magnetic field in the wall region ($r > r_w$) is dominated by the exponential factor since $\delta << r_w$. Thus, in imposing condition (A10), we can ignore the geometrical factor $r^{-1/2}$ in Eq. (A8). It can then immediately be shown that (A9) and (A10) lead to the dispersion relationship

$$\frac{\delta}{r_w}\left[\frac{1-i}{2}\right](k_{n1}r_w)\,J_0(k_{n1}r_w) = J_1(k_{n1}r_w) \tag{A11}$$

which is reproduced as Eq. (4) in the main text. Of course, this dispersion relation can also be obtained by first formulating the field solutions in the wall region in terms of Bessel functions (with complex arguments), to be followed by the use of asymptotic formulas of the Bessel functions when $\delta/r_w << 1$. The formulation presented above illustrates clearly the nature of such approximations.

With $\zeta \equiv k_{n1} r_w$ and $\delta/r_w << 1$, Eq. (A11) admits the approximate solution

$$\zeta = \zeta_{on} + \Delta\zeta \tag{A12}$$

where $J_1(\zeta_{on}) = 0$ and $\Delta\zeta$ is given by

$$\Delta\zeta = \frac{(\delta/r_w)\left|\frac{1-i}{2}\right|\zeta_{on} J_0(\zeta_{on})}{(\partial J_1(\zeta)/\partial\zeta)_{\zeta=\zeta_{on}}}. \tag{A13}$$

Equation (A12) reduces to Eq. (6) of the main text after we use in (A13) the formula $\partial J_1(\zeta)/\partial\zeta = J_0(\zeta)$ at the roots ζ_{on} of J_1.

We summarize by stating that the vacuum fields of the TE_{on} mode in a lossy waveguide are given by Eqs. (1)-(3) in the main text. The radial wavenumber α_n in these expressions is given by Eq. (7). The influence of the wall resistivity on the beam dynamics will be discussed in Appendix B.

Appendix B

EFFECTS OF RESISTIVE WALL ON THE DYNAMICS OF THE ELECTRON BEAM

In this Appendix, we assess the influence on the electron beam dynamics by a small, but finite, wall resistivity. We shall show (a) that the loss in the forward gain of the amplifier is approximately 1/3 of the cold tube loss and (b) that the electron beam essentially experiences the vacuum field inside a *lossless* waveguide. Again, our estimates will be based on the smallness of δ/r_w and we shall consider complex roots of k_z for real values of ω.

Near synchronism, $\omega^2 - k_z^2c^2 - \alpha_n^2c^2 \simeq 0$ and $\omega - k_z v_{zo} - s\Omega_c \simeq 0$. The second term in the right hand member of Eq. (16) can be ignored compared with the first term. We can further approximate $\omega^2 - k_z^2c^2$ by $\alpha_n^2c^2$ in the right hand side of (16). Thus, Eq. (16) is simplified to read

$$(\omega^2 - k_z^2\, c^2 - \alpha_n^2c^2)\ (\omega - k_z v_{zo} - s\Omega_c)^2 = -\frac{4\nu\alpha_n^4c^4\beta_{\perp o}^2}{\gamma_o\, \zeta_{on}^2\, J_0^2\,(\zeta_{on})}\, H_s(\alpha_n r_o;\, \alpha_n r_L) \tag{B1}$$

where, for analytical tractability, we have set $\Delta p_z = 0$.

With $\bar{\omega} \equiv \omega r_w/c$, $\bar{k} \equiv k_z r_w$, Eq. (B1) becomes

$$\left\{\bar{k}^2 - \bar{\omega}^2 + \zeta_{on}^2\left[1 + \frac{\delta}{r_w}\,(1-i)\right]\right\}\left[\bar{k} - \frac{\bar{\omega} - \bar{\Omega}_c}{\beta_{\parallel}}\right]^2 = E \equiv E_r + iE_i \tag{B2}$$

where we have used Eq. (7) and $\bar{\Omega}_c \equiv s\Omega_c r_w/c$. In Eq. (B2), the parameter E, whose real and imaginary parts are denoted E_r and E_i, is proportional to the right hand member of Eq. (B1). It is clear from (7) and (B1) that

$$\frac{E_i}{E_r} = 0\left(\frac{\delta}{r_w}\right). \tag{B3}$$

Thus, both sides of (B2) are modified by wall resistivity through the introduction of a term of order δ/r_w. The statement (b) at the beginning of this Appendix claims that E_i can be neglected. The argument supporting this claim will be given later in the Appendix. We shall now prove the statement (a).

In the absence of the beam, $E \to 0$, and the wave inside the lossy waveguides attenuates at a rate given by the imaginary part of $\bar{k}_w$, where

$$\bar{k}_w = \bar{\omega}^2 - \zeta_{on}^2 \left[1 + \frac{\delta}{r_w}(1-i)\right]^{1/2} \simeq (\bar{\omega}^2 - \zeta_{on}^2)^{1/2}\left[1 + \frac{\zeta_{on}^2 (i-1)\,\delta/r_w}{2(\bar{\omega}^2 - \zeta_{on}^2)}\right]. \tag{B4}$$

The last expression is valid once $\bar{\omega}/\zeta_{on} - 1 > \delta/r_w$, i.e., once the frequency ω exceeds the cut-off frequency ω_c by the (small) amount $(\delta/r_w)\omega_c$. Thus the normalized attenuation rate of the cold tube is

$$Im(\bar{k}_w) \cong \zeta_{on}^2 \left|\frac{\delta_c}{2r_w}\right| \Big/ (\bar{\omega}^2 - \zeta_{on}^2)^{1/2}. \tag{B5}$$

To estimate the reduction of the gain by the wall resistivity, we neglect E_i in (B2) and rewrite (B2) as

$$(\bar{k} - \bar{k}_w)\,(\bar{k} - \bar{k}_B)^2 = \frac{E}{(\bar{k} + \bar{k}_w)} \tag{B6}$$

where

$$\bar{k}_B = \frac{\bar{\omega} - \bar{\Omega}_c}{\beta_{\|}}, \tag{B7}$$

which is real for real values of $\bar{\omega}$. If we consider the vicinity of the grazing condition, at which

$$\bar{k}_B \equiv \frac{\bar{\omega} - \bar{\Omega}_c}{\beta_{\|}} \simeq (\bar{\omega}^2 - \zeta_{on}^2)^{1/2}, \tag{B8}$$

then we may rewrite Eq. (B6) as

$$\bar{k}'^2\,[\bar{k}' + (\bar{k}_B - \bar{k}_w)] = \frac{E}{(\bar{k} + \bar{k}_w)} \simeq \frac{E}{2\bar{k}_g} \equiv E_1 \tag{B9}$$

where we have defined

$$\bar{k}' \equiv \bar{k} - \bar{k}_B \tag{B10}$$

and $\bar{k}_g \equiv \zeta_{on}\beta_{\|}\,(1-\beta_{\|}^2)^{-1/2}$ is the characteristic wavenumber at the grazing condition. Note that $\mathrm{Im}(\bar{k}') = \mathrm{Im}(\bar{k})$. Upon using (B8) and (B4), we have

$$\bar{k}_B - \bar{k}_w \simeq -\frac{\zeta_{on}^2}{2}\left(\frac{\delta}{r_w}\right)\frac{(i-1)}{(\bar{\omega}^2 - \zeta_{on}^2)^{1/2}}. \tag{B11}$$

Equation (B11) may now be used in Eq. (B9) to estimate the effect of a small (δ/r_w) on the gain per unit length, which is measured by the imaginary part of $\bar{k}'$. We represent the solutions to Eq. (B9) as

$$\bar{k}' = \bar{k}'_0 + \bar{k}'_1. \tag{B12}$$

where $\bar{k}'_0$ is the solution to (B9) when wall resistivity is absent, (i.e., $\delta = 0$). Thus, $\bar{k}'_0$ satisfies

$$\bar{k}'^3_0 = E_1 \tag{B13}$$

and the imaginary part of $\bar{k}'_1$ represents the reduction of the forward gain by the wall loss. By substituting (B12) into (B9) and by assuming $\bar{k}'_1 << \bar{k}'_0$, we obtain

$$\bar{k}'_1 \simeq -\frac{1}{3}(\bar{k}_B - \bar{k}_w) \simeq \frac{\zeta_{on}^2}{6} \frac{(\delta/r_w)(i-1)}{\sqrt{\bar{\omega}^2 - \zeta_{on}^2}} \tag{B14}$$

whose imaginary part is approximately 1/3 of $\mathrm{Im}(\bar{k}_w)$ by Eq. (B4). These qualitative estimates are confirmed by detailed numerical calculations (c.f. Fig. (4)). Thus, the reduction in the forward gain because of the wall resistivity is only one third of the cold tube loss.

We finally show that a small imaginary part in the RHS of the dispersion relationship (B2) [or (B9)] has a negligible influence on the gain. To this end, let us consider Eq. (B9) and add a small imaginary part to its right hand side. Then (B9) becomes

$$\bar{k}'^2 [\bar{k}' + \delta_1] = \bar{k}'^3_0 (1 + i\delta_2) \tag{B15}$$

where δ_1 and δ_2 are both of the order of δ/r_w and $\bar{k}'^3_0 = E_1$. Again, expressing the approximate solution to (B15) in the form of (B12), we find

$$\bar{k}'_1 \simeq -\frac{1}{3}[\delta_1 - i\bar{k}'_0 \delta_2]. \tag{B16}$$

Since δ_1 and δ_2 are of the same order and $\bar{k}'_0 = E_1^{1/3}$ is a small quantity whose order of magnitude is typically in the range between 0.01 and .1, we conclude that the introduction of a small imaginary part in the RHS of the dispersion relation (16) has a much smaller effect than that appearing on the LSH of (16). In physical terms, the modified fields by the wall resistivity does not significantly affect the beam current perturbation in response to these fields.

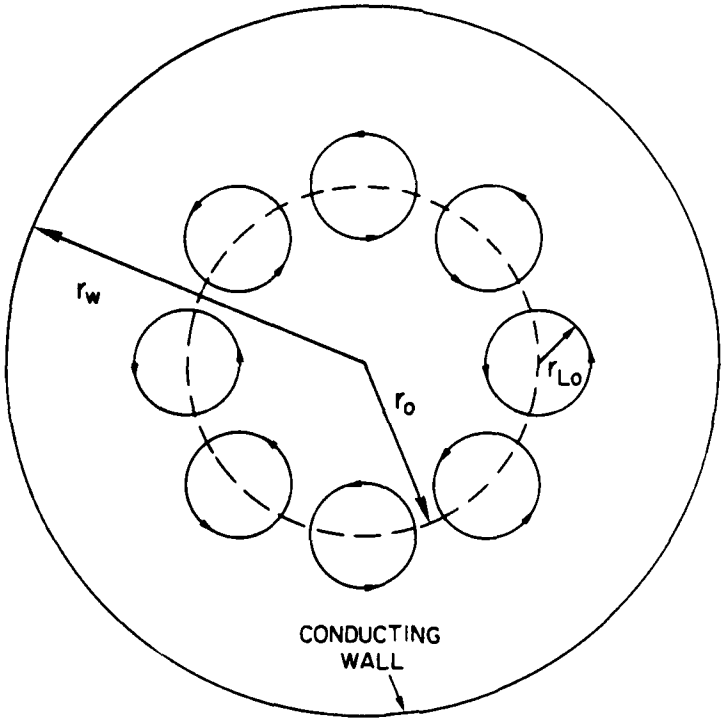

Fig. 1 — Cross sectional view of the gyro-TWA. The applied magnetic field points out of the paper.

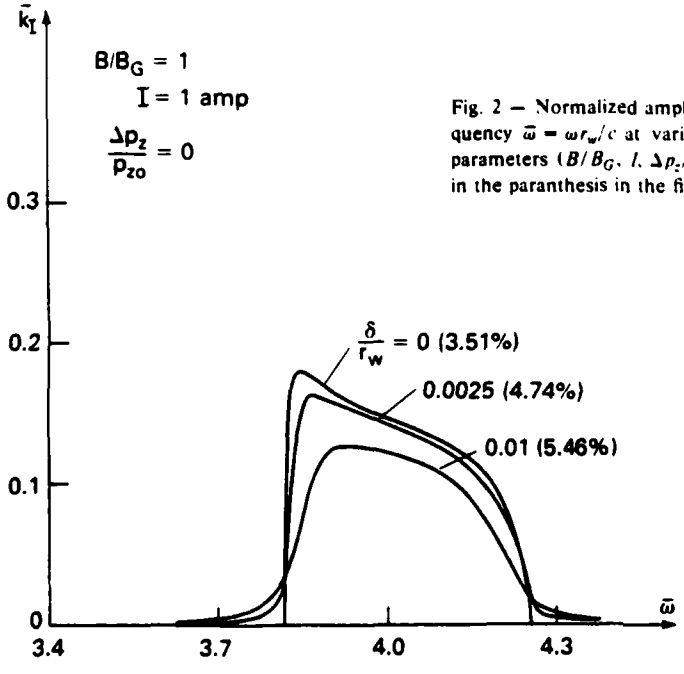

Fig. 2 — Normalized amplification rate $\bar{k}_I = |k_I| r_w$ versus normalized frequency $\bar{\omega} = \omega r_w/c$ at various values of wall resistivity (δ/r_w). All other parameters $(B/B_G, I, \Delta p_z/p_{zo})$ are fixed as indicated. The numbers shown in the paranthesis in the figure denote the bandwidths.

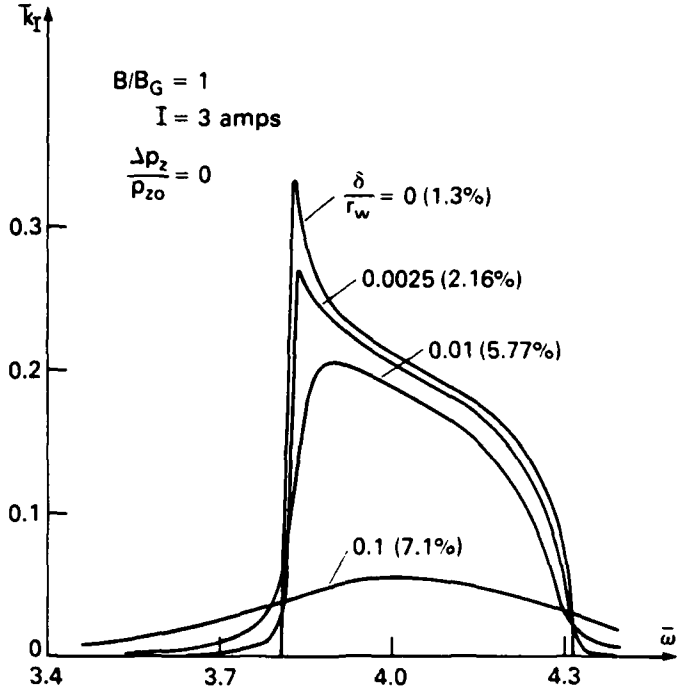

Fig. 3 — Same as in Fig. 2.

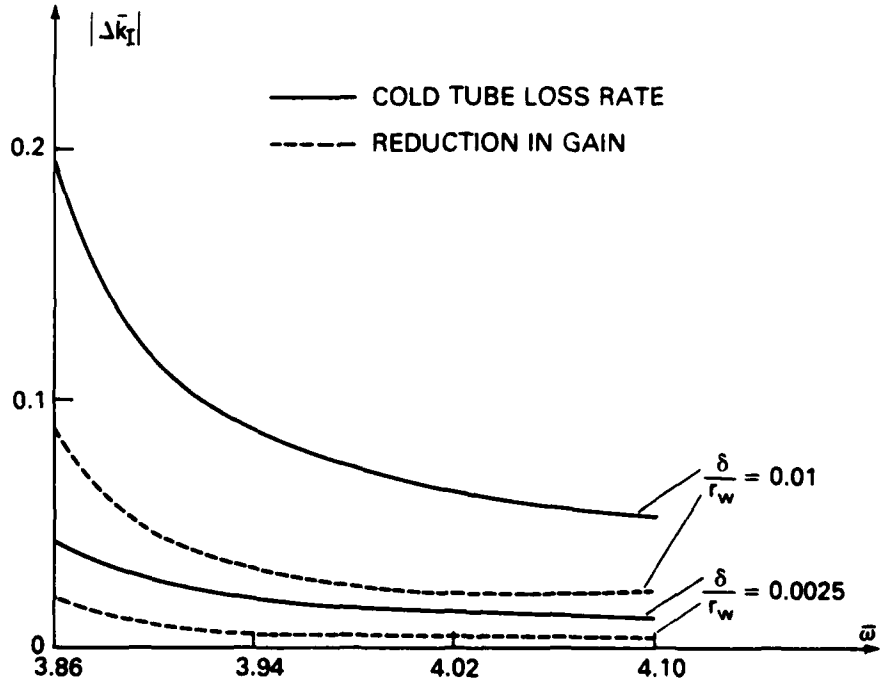

Fig. 4 — Cold tube loss rate (solid curves) and the reduction in the amplification rate (dashed curves) due to wall resistivity. The parameters for the dashed curves are $B/B_G = 1$, $\Delta\rho_z = 0$, $I = 1$ amp. The same dashed curves are obtained if I is raised to 3 amps.

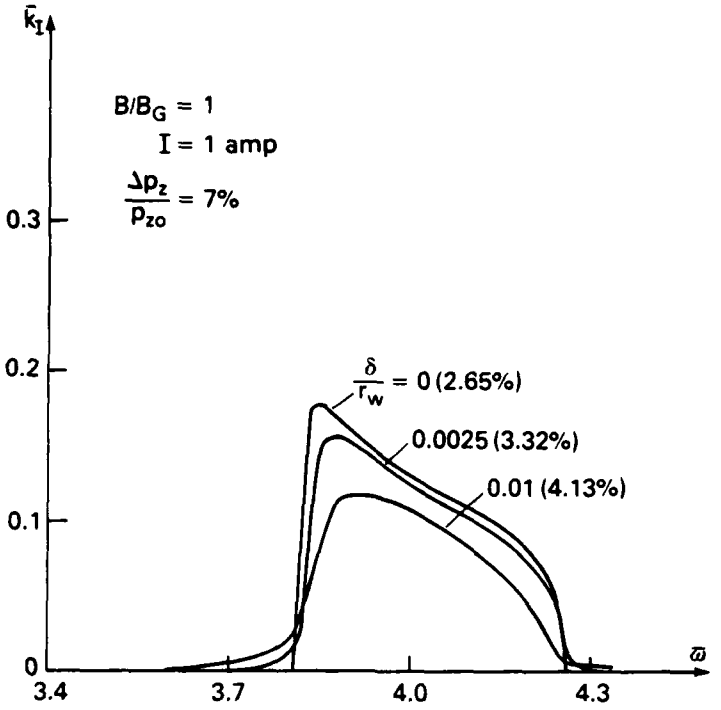

Fig. 5 — Same as in Fig. 2.

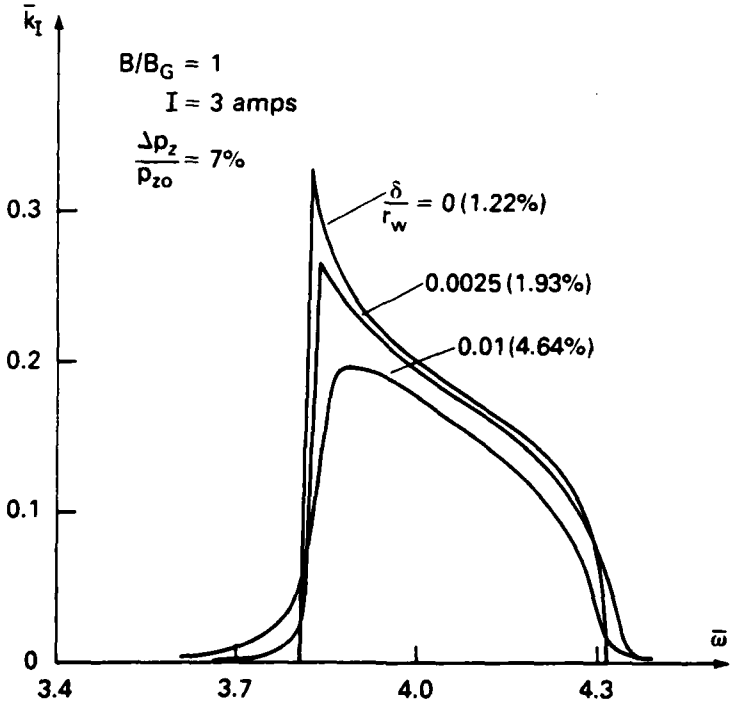

Fig. 6 — Same as in Fig. 2.

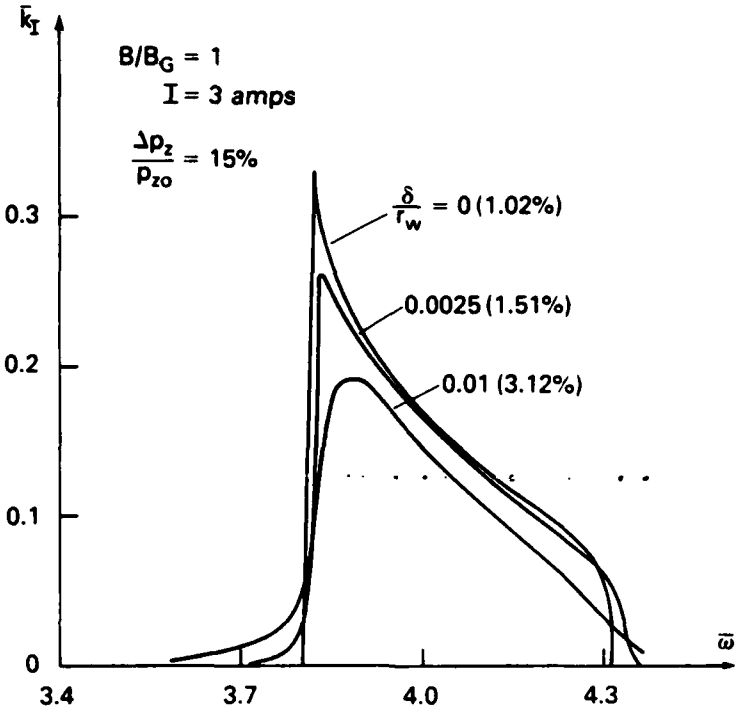

Fig. 7 — Same as in Fig. 2.

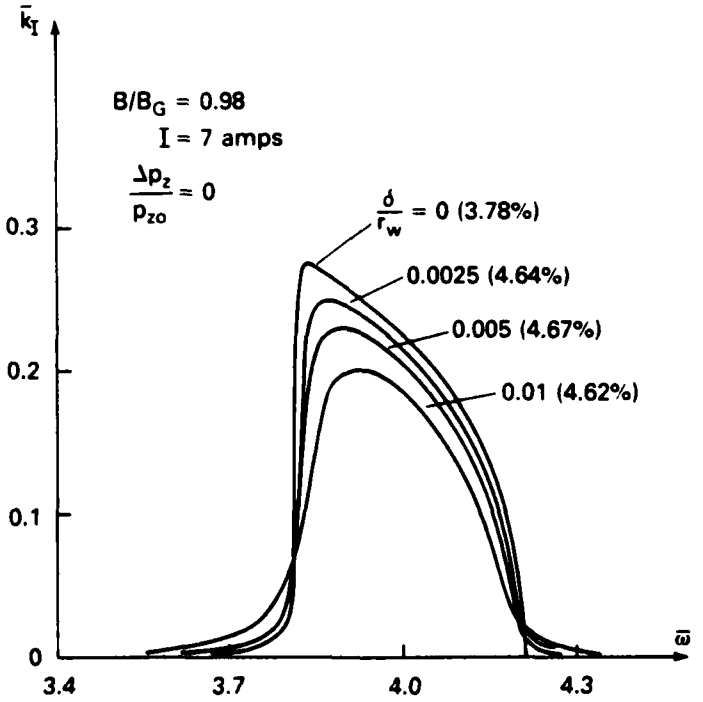

Fig. 8 — Same as in Fig. 2.

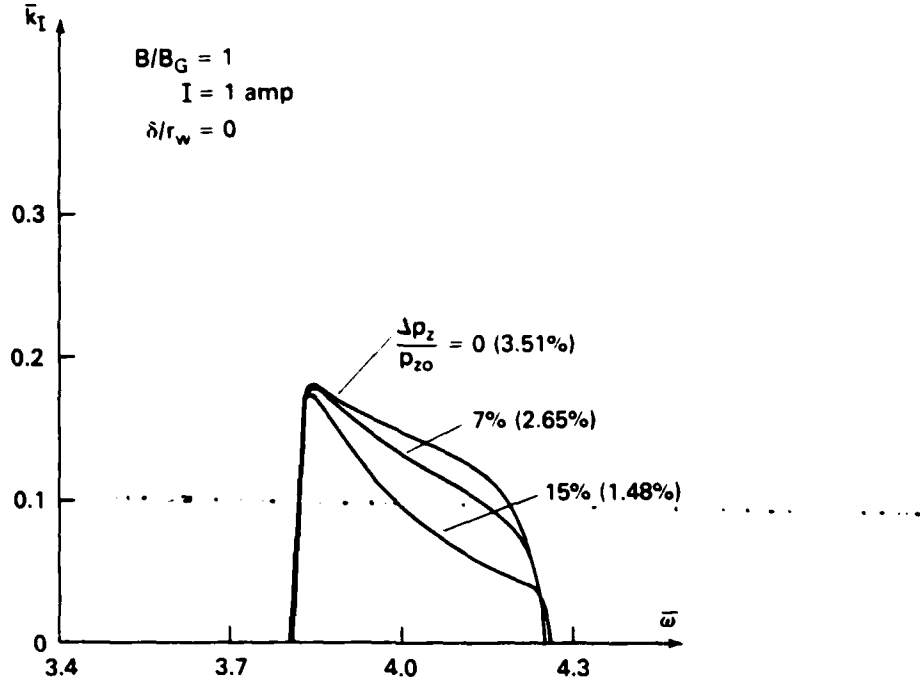

Fig. 9 — Normalized amplification rate $\bar{k}_I$ versus normalized frequency $\bar{\omega}$. Here, only the velocity spread $\Delta p_z/p_{zo}$ is allowed to vary, all other parameters (B/B_G, I, δ/r_w) are fixed at the values as indicated in the figure. The numbers in paranthesis denote the bandwidth.

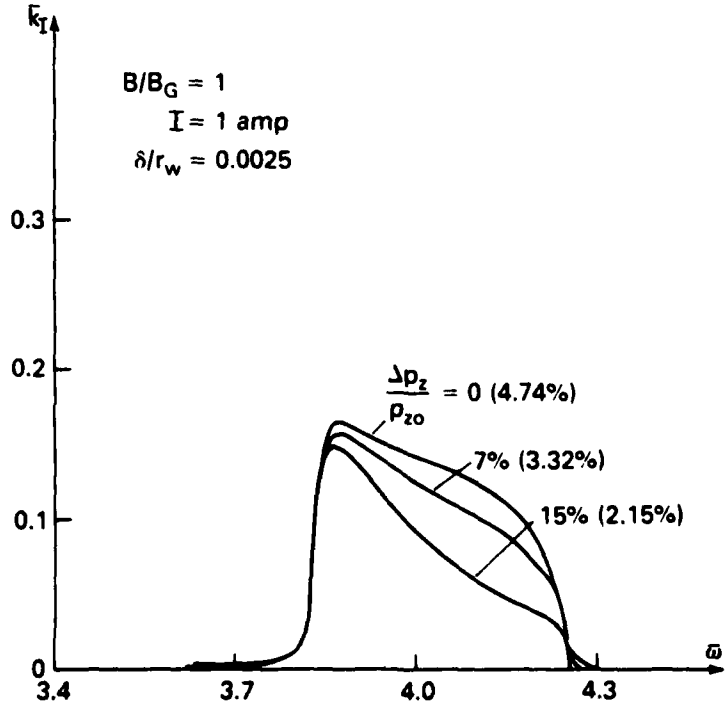

Fig. 10 — Same as in Fig. 9

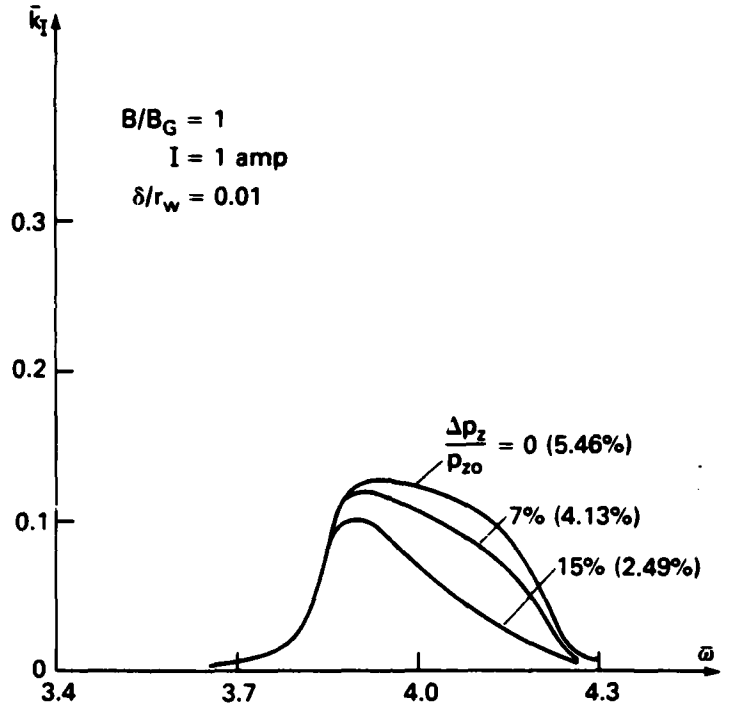

Fig. 11 — Same as in Fig. 9.

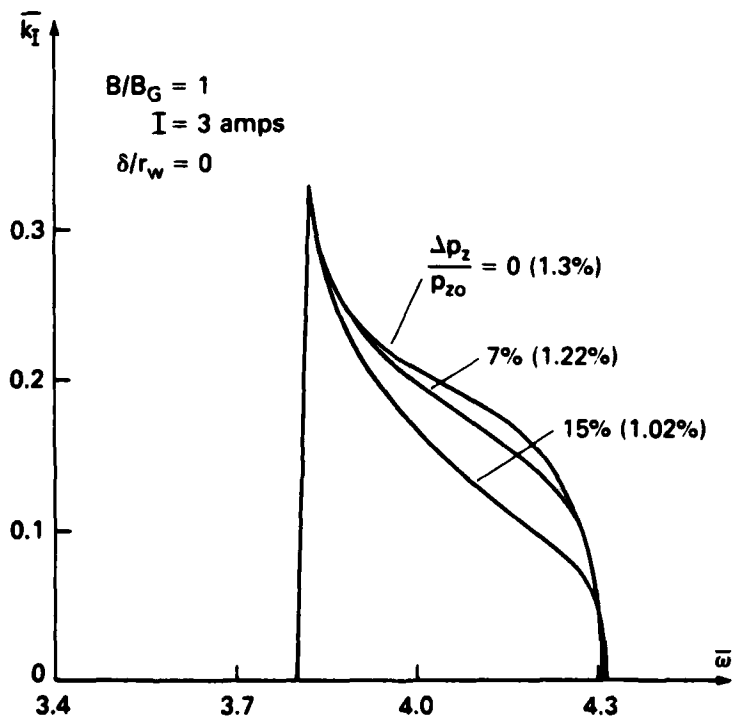

Fig. 12 — Same as in Fig. 9.

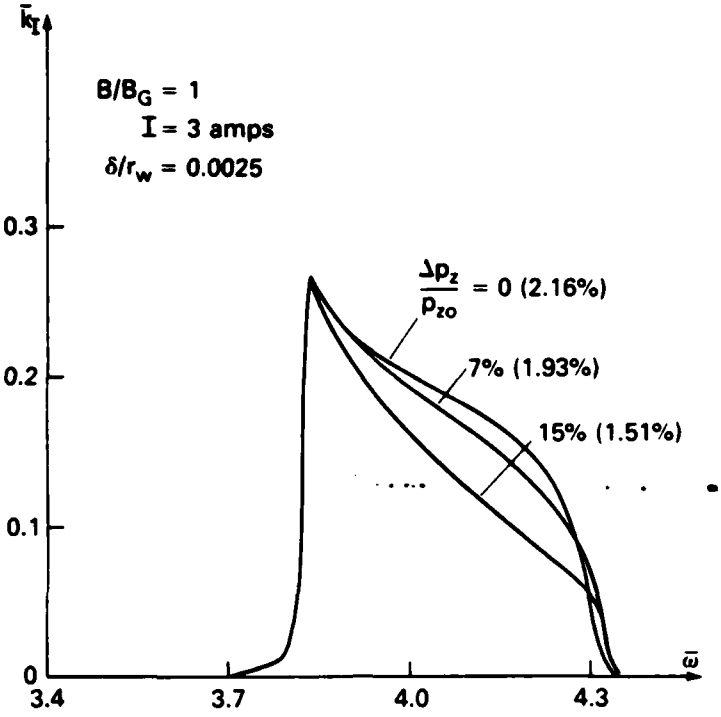

Fig. 13 — Same as in Fig. 9.

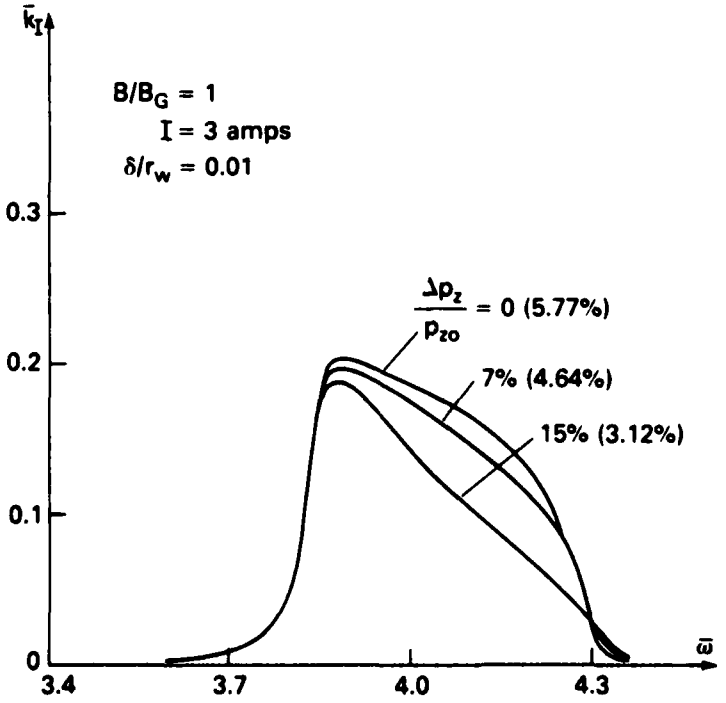

Fig. 14 — Same as in Fig. 9.

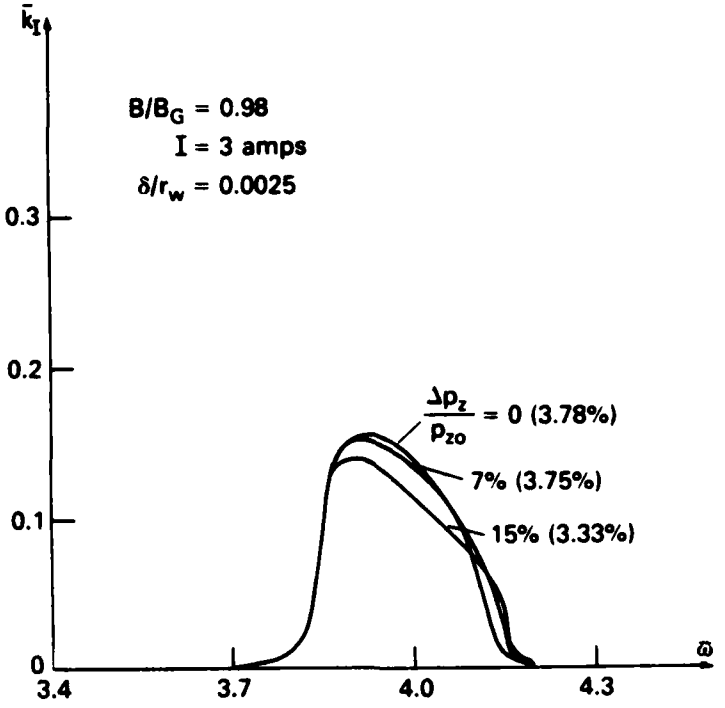

Fig. 15 — Same as in Fig. 9.

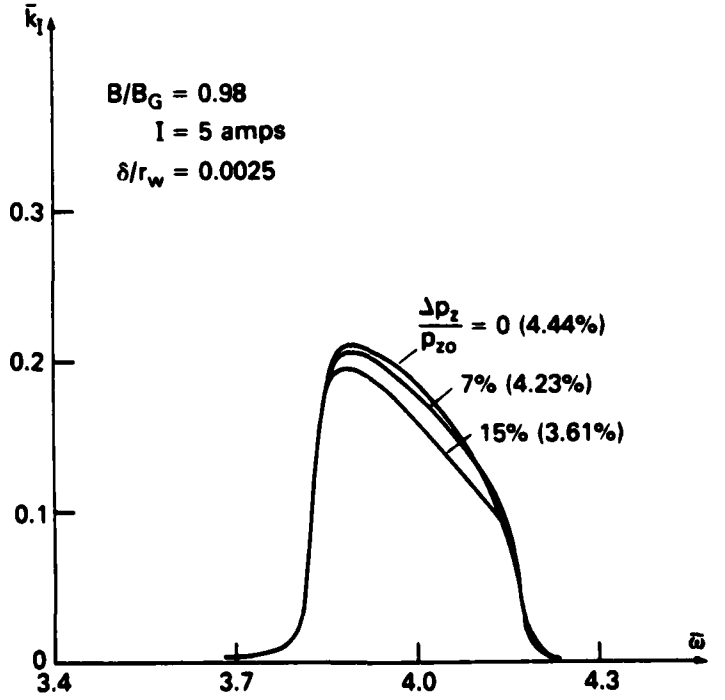

Fig. 16 — Same as in Fig. 9.

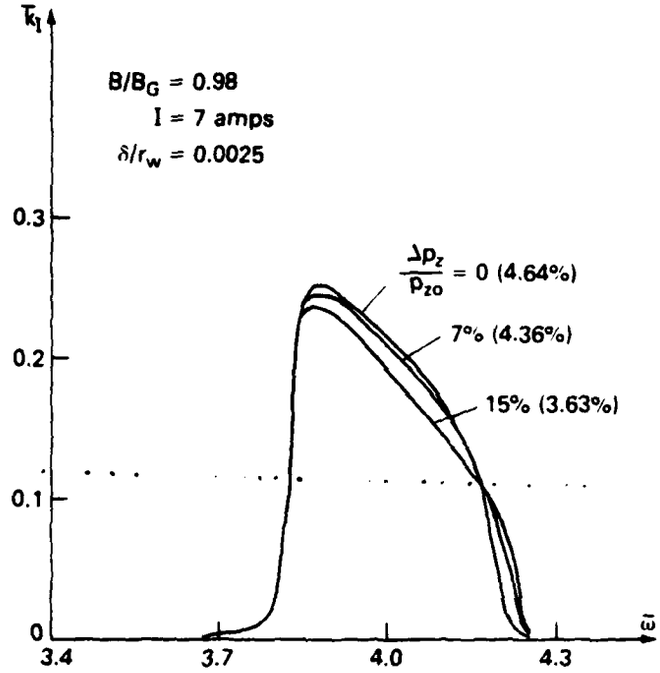

Fig. 17 — Same as in Fig. 9.

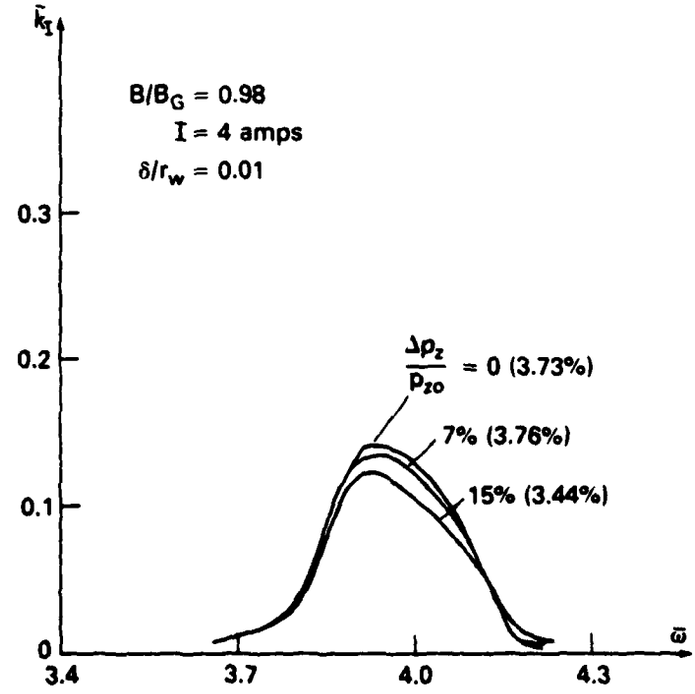

Fig. 18 — Same as in Fig. 9.

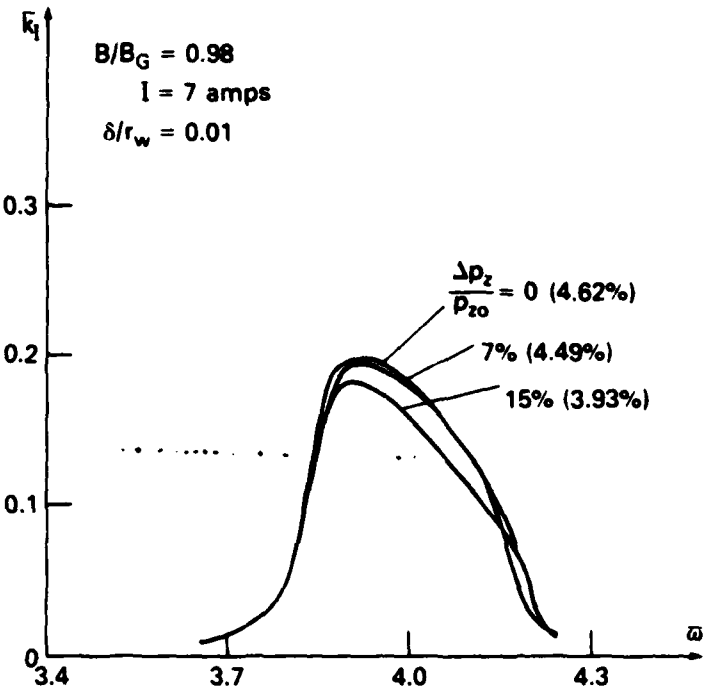

Fig. 19 — Same as in Fig. 9.

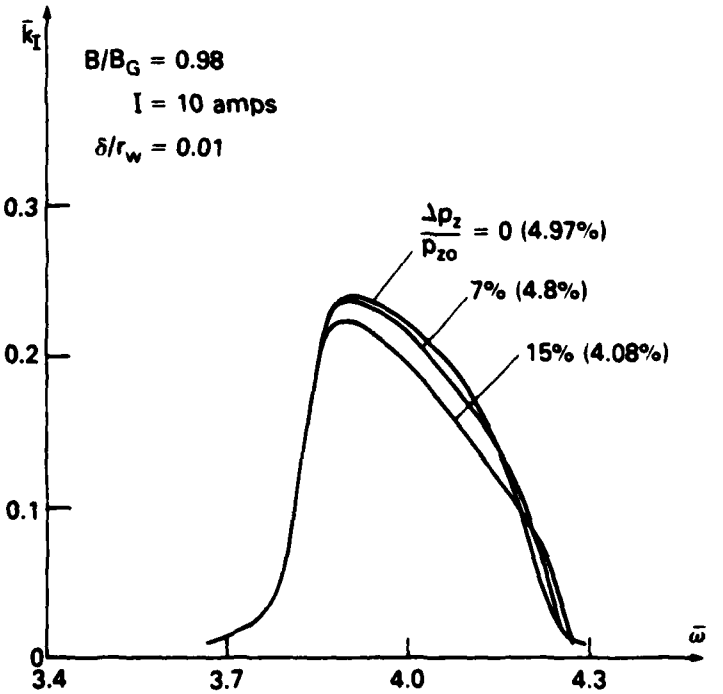

Fig. 20 — Same as in Fig. 9.

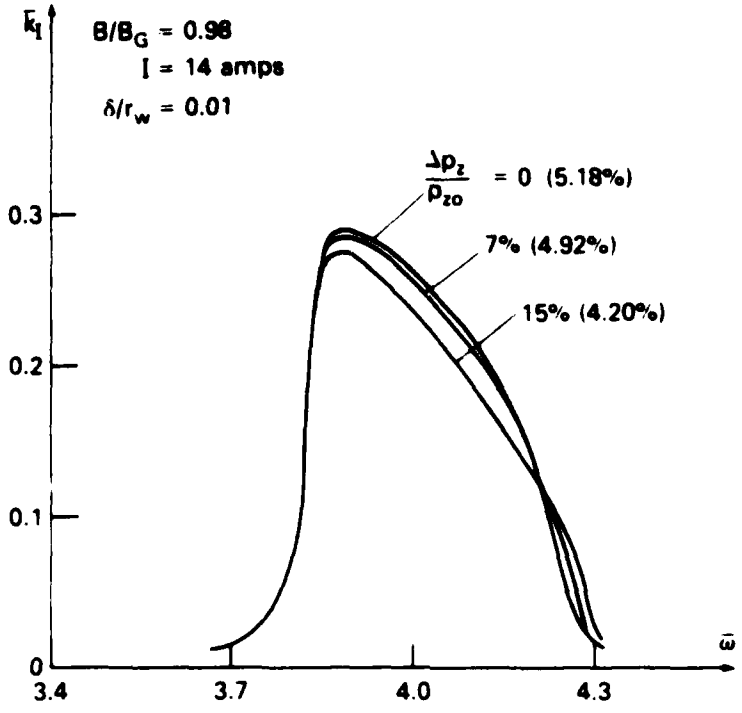

Fig. 21 — Same as in Fig. 9

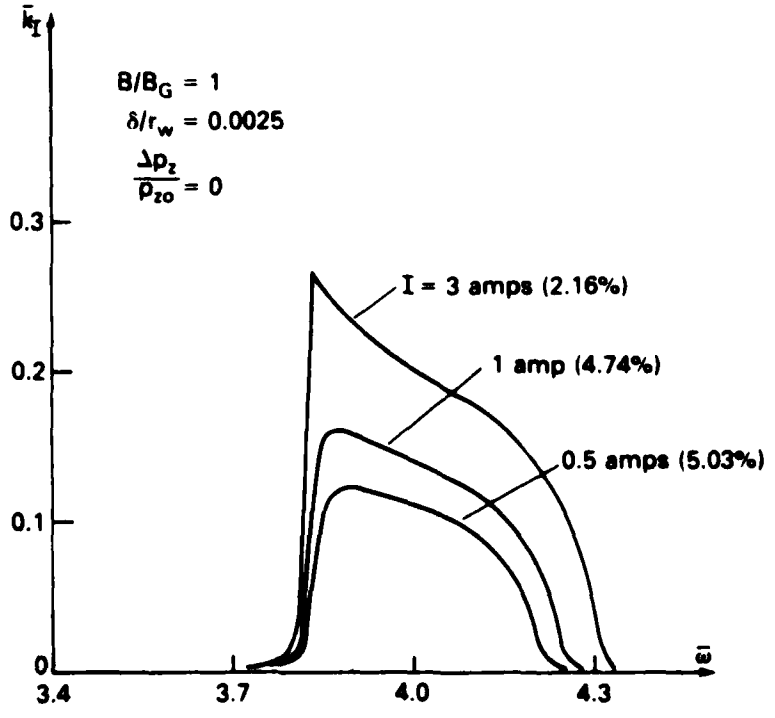

Fig. 22 — Normalized amplification rate $\bar{k}_I$ versus normalized frequency $\bar{\omega}$. Here, only the current I is allowed to vary, all other parameters B/B_G, δ/r_w, $\Delta p_z/p_{zo}$) are fixed at the values as indicated in the figure. The numbers in paranthesis denote the bandwidths

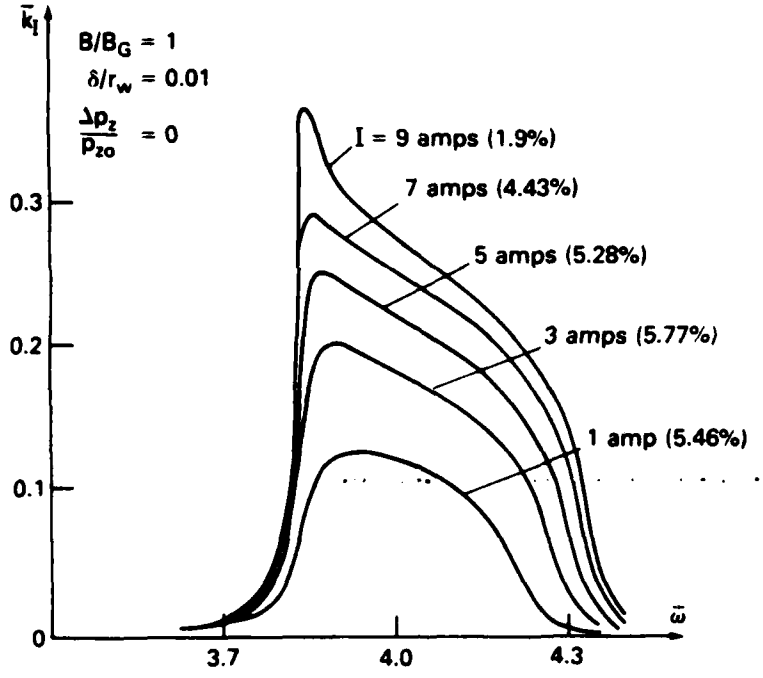

Fig. 23 — Same as Fig. 22.

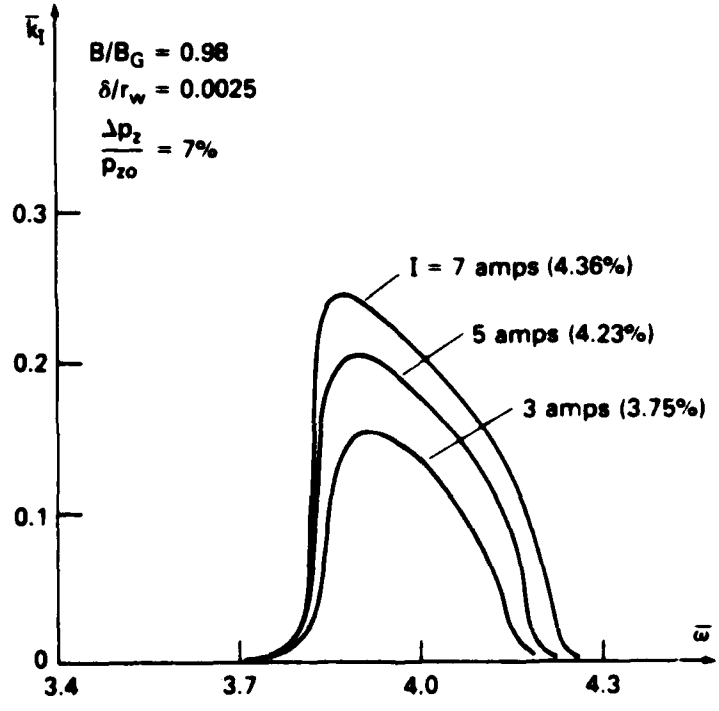

Fig. 24 — Same as Fig. 22

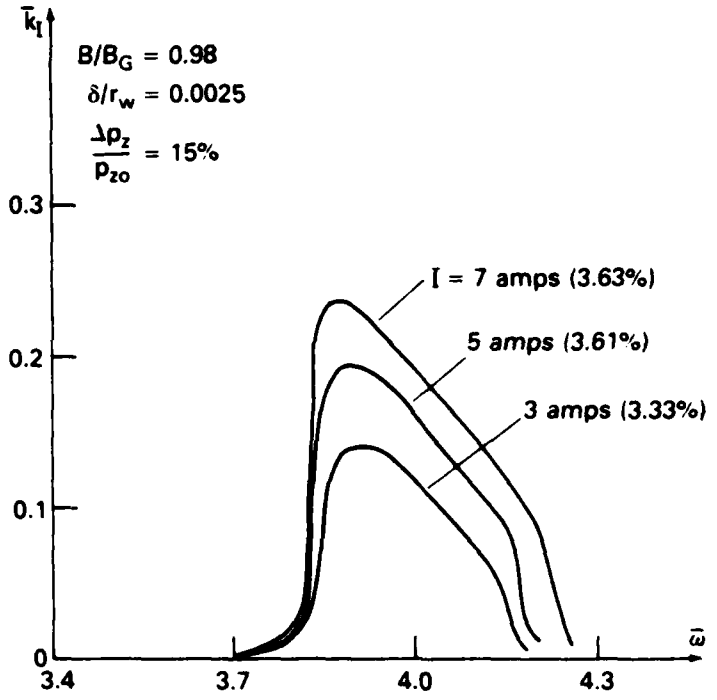

Fig. 25 — Same as Fig. 22.

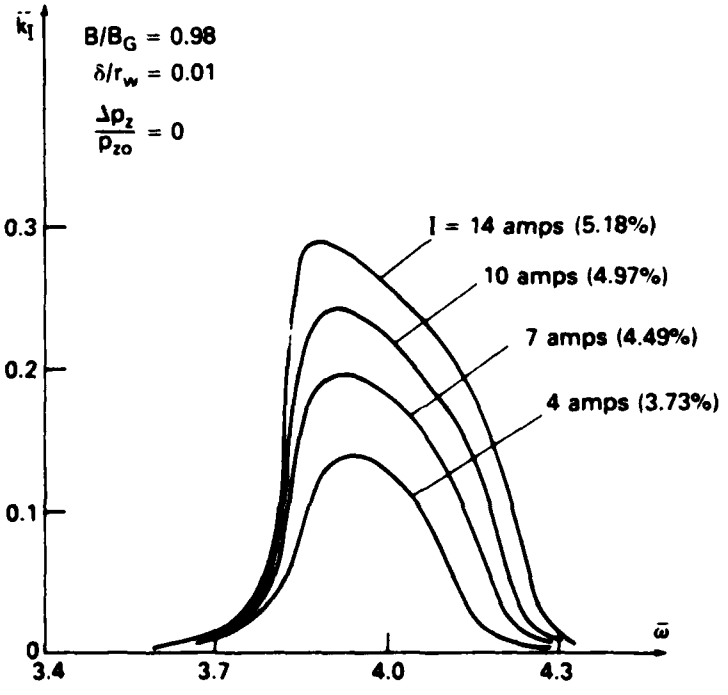

Fig. 26 — Same as Fig. 22

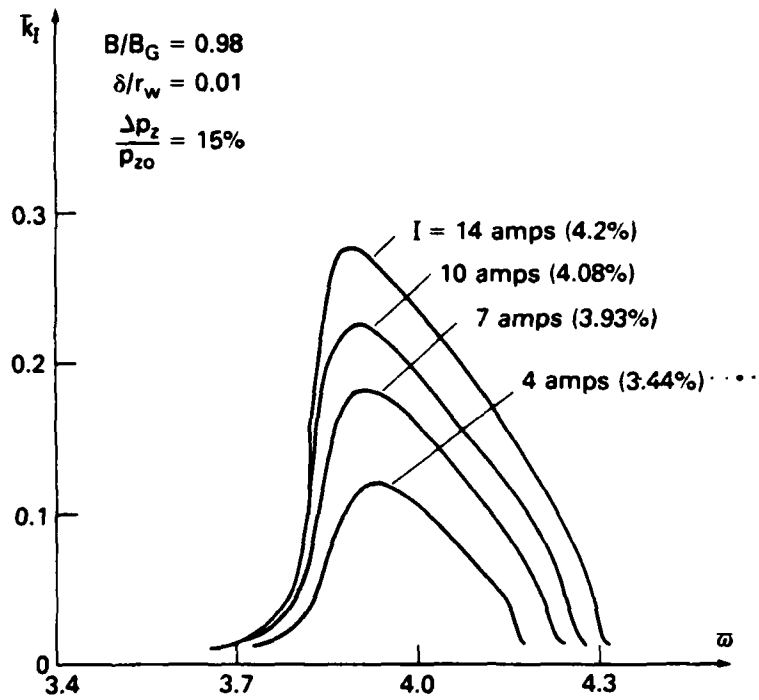

Fig. 27 — Same as Fig. 22.

GYROTRON & ECH DISTRIBUTION LIST

No. of Copies			Addressee
(25) (26)	Naval Research Laboratory Attn: Name/Code 4555 Overlook Avenue, S.W. Washington, D.C. 20375	Code:	4700 - Dr. T. Coffey 4740 - Dr. V.L. Granatstein 4740 - Dr. R.K. Parker 4740 - Dr. K.R. Chu 4740 - Dr. M.E. Read 4740 - Dr. C.W. Roberson 4740 - Dr. S. Gold 4790 - Dr. P.A. Sprangle 4790 - Dr. B. Hui 4790 - Dr. W.M. Manheimer 6850 - Dr. L.R. Whicker 6853 - Dr. A. Ganguly 6805 - Dr. S.Y. Ahn 6805 - N.R. Vanderplaats 6875 - Dr. R. Wagner
	On-Site Contractors:	Code:	4740 - Dr. J.M. Baird (B-K Dynamics) 4740 - Dr. L. Barnett (B-K Dynamics) 4740 - Dr. D. Dialetis (SAI) 4740 - A.J. Dudas (JAYCOR) 4740 - Dr. R.M. Gilgenbach (JAYCOR) 4740 - Dr. K.J. Kim (JAYCOR) 4740 - Dr. Y.Y. Lau (SAI) 4740 - Dr. J.S. Silverstein (HDL) 4790 - Dr. A.J. Drobot SAI) 4790 - Dr. C.M. Hui (JAYCOR) 4790 - Dr. J. Vomvoridis (JAYCOR) 5704S - Dr. S. Smith (LOCUS, Inc.)
(3)	Secretary Department of Energy Attn: Washington, D.C. 20545		Dr. P. Stone (G-234) Dr. M. Murphy (G-234) Dr. J. Willis (G-234)
(1)	Air Force Avionics Laboratory Attn: W. Friz Wright/Patterson AFB, Ohio 45433		
(1)	Bell Laboratories Attn: Dr. W.M. Walsh, Jr. 600 Mountain Avenue Murray Hill, New Jersey 07971		

No. of Copies		Addressee
(1)	Columbia University Department of Electrical Engineering Attn: Dr. S.P. Schlesinger New York, New York 10027	
(1)	Dartmouth College Physics Department Attn: Dr. John Walsh Dartmouth, New Hampshire 03755	
(12)	Defense Technical Information Center Cameron Station 5010 Duke Street Alexandria, Virginia 22314	
(1)	Georgia Institute of Technology Engineering Experimental Station Attn: Dr. James J. Gallagher Atlanta, Georgia 30332	
(3)	Hughes Aircraft Co. Attn: Electron Dynamics Division 3100 Lomita Boulevard Torrance, California 90509	Dr. J.J. Tancredi K. Arnold K. Amboss
(1)	Los Alamos Scientific Laboratory Attn: Dr. Paul Tallerico P.O. Box 1663 Los Alamos, New Mexico 87545	
(1)	Massachusetts Institute of Technology Research Laboratory of Electronics Attn: Dr. G. Bekefi Bldg. 36, Rm. 36-225 Cambridge, Massachusetts 02139	
(3)	Massachusetts Institute of Technology Plasma Fusion Center Attn: 167 Albany St., N.W. 16-200 Cambridge, Massachusetts 02139	Dr. R. Davidson Dr. M. Porkolab Dr. R. Temkin
(1)	Northrop Corporation Defense System Department Electronics Division Attn: G. Doehler 175 W. Oakton St. Des Plaines, Illinois 60018	
(2)	Oak Ridge National Laboratories Attn: P.O. Box Y Oak Ridge, Tennessee 37830	Dr. A. England M. Loring

No. of Copies		Addressee
(1)	Princeton University Plasma Physics Laboratory Attn: Dr. H. Hsuan Princeton, New Jersey 08540	
(2)	Raytheon Company Microwave Power Tube Division Attn: Willow St. Waltham, Massachusetts 02154	R. Edwards R. Handy
(1)	Science Applications, Inc. Attn: Dr. Alvin Trivelpiece 1200 Prospect St. La Jolla, California 92037	
(1)	Stanford University SLAC Attn: Dr. Jean Lebacqz Stanford, California 94305	
(1)	University of Arizona Optical Sciences Center Attn: Dr. W.E. Lamb Tucson, Arizona 85720	
(1)	Varian Associates Bldg. 1 Attn: Dr. H. Jory 611 Hansen Way Palo Alto, California 94303	
(1)	Yale University Mason Laboratory Attn: Dr. J.L. Hirshfield 400 Temple Street New Haven, Connecticut 06520	
(1)	Kings College University of London Attn: Dr. P. Lindsay London, United Kingdom	
(1)	Nagoya University Institute of Plasma Physics Attn: Dr. H. Ikegami Nagoya, Japan 464	
(1)	National Taiwan University Department of Physics Attn: Dr. Yuin-Chi Hsu Taipei, Taiwan, China	

No. of Copies	Addressee
(1)	TFR Group DPH - PFC Attn: Dr. A. Cavallo 92260 Fontenay-auix Roses France
(1)	Thompson C.S.F./DET/TDH Attn: Dr. G. Mourier 2 Rue Latecoere 78140 Velizy Villa conblay France
(1)	UKAEA Culham Laboratory Attn: Dr. A.C. Riviere Abingdon Oxfordshire United Kingdom